

Organic ultraviolet photodetectors based on subphthalocyanine derivatives

L. Zhou, F. Ma*, G. Zhang, J. Tian, Y. Zhang, J. Zhao, B. Hu

School of Chemistry and Chemical Engineering, Tianjin University of Technology, Tianjin 300384

In this article, four subphthalocyanine (SubPc) derivatives were synthesized and characterized. These materials exhibit strong ultraviolet (UV) absorption and excellent donor properties, as confirmed by photophysical and electrochemical characterization. Solution-processed UV photodetectors incorporating SubPc 3a (shown in Scheme 1) as the active layer demonstrate outstanding performance, achieving an external quantum efficiency (EQE) of 38.76 % and a specific detectivity (D^*) of 2.18×10^{12} Jones. This work provides valuable insights into structure-property relationships of SubPc derivatives and advances their application in UV detection technologies.

(Received March 18, 2025; Accepted June 21, 2025)

Keywords: Sensitive, UV photodetector, Subphthalocyanine derivatives

1. Introduction

Ultraviolet (UV) photodetectors play a critical role in a wide range of applications, including defense early warning systems, UV communication, space exploration, environmental monitoring, industrial processes, medical diagnostics, biochemical sensing, and healthcare [1-3]. The current market for UV photodetectors is dominated by three primary material categories: organic, inorganic, and organic-inorganic hybrid semiconductors. Among these, inorganic semiconductors such as SiC, GaN, and ZnO-based materials have become really popular because of their great properties, including low defect density, high carrier drift velocity, and robust radiation resistance, making them perfect for even the most demanding applications [4-5]. Organic semiconductors have also emerged as viable candidates for UV photodetection. For instance, 3, 6-dipyrenyl-N-hexylcarbazole (P2NHC) has demonstrated promising performance as an active layer, achieving an internal quantum efficiency of 64% [6]. Meanwhile, organic-inorganic hybrid materials have recently caught people's attention as being really promising for use in optoelectronic devices. A notable example is the inorganic hybrid perovskite (MV) $[\text{SbI}_3\text{Cl}_2]$, which has been utilized in UV photodetectors with an EQE of 6.69%. Despite significant advances in the development and application of photodetection materials, significant challenges remain, including limited solubility, high production costs, low stability, complex fabrication processes, environmental concerns, and difficulties in achieving uniform film formation. These limitations hinder the widespread adoption of these materials [7]. Consequently, ongoing research efforts are focused on developing novel materials to address these issues.

*Corresponding author: mafontune@sina.com.cn

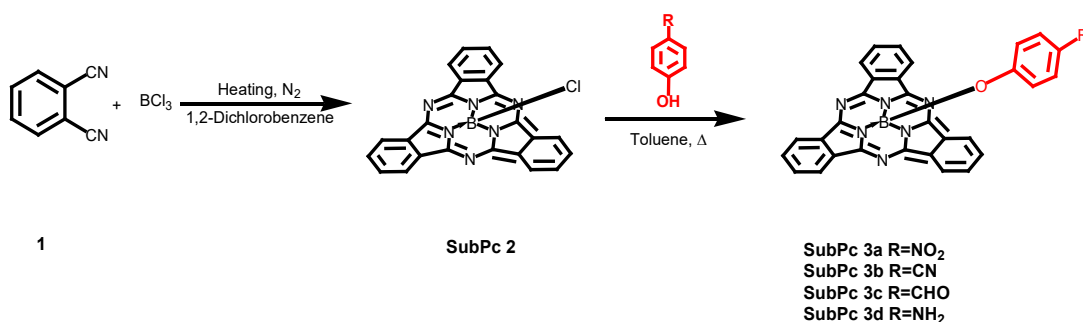
Subphthalocyanines (SubPcs) have attracted considerable interest due to their unique planar macrocyclic structure, which consists of three isoindole subunits coordinated to a central boron atom [8]. This configuration creates a conjugated system with 14 π -electrons [9-10], enabling strong absorption in the UV B-band and visible Q-band regions. Their simple synthesis and versatile properties have led to their use in organic photodetectors (OPDs) [11], light-emitting diodes [12-13], solar cells [14-15], and photodynamic therapy, among others. In the field of OPDs, Jin et al. [9] have developed an OPD based on SubPcBr, which exhibits high detectivity and external quantum efficiency (EQE). While the absorption properties of subphthalocyanines in the Q-band have been well studied, leading to the development of sensitive green-light photodetectors, their B-band absorption for organic photodetection has not been explored yet.

This study reports the synthesis of four new subphthalocyanine derivatives, with a detailed analysis of their photophysical, electrochemical, and thermal properties. UV photodetectors with high sensitivity were prepared from these SubPc compounds using a solution-based process. Especially, the device containing SubPc 3a (shown in Scheme 1) achieved an EQE of 38.76 %, a D^* of 2.18×10^{12} Jones, and a τ of about 32 ms at 0 bias under 320 nm UV light exposure. Also, impedance spectroscopy was used to measure the conductivity of these SubPc materials.

2. Experimental

2.1. Synthesis

The SubPc derivatives were synthesized following the procedure outlined in Scheme 1. SubPc 2 (Cl-BSubPc) was prepared using methods described by Pieter J. Swarts et al. [16]. According to the synthetic methods already available in our group, the nucleophilic substitution reaction of SubPc 2 with phenol derivatives gave the target products SubPc 3a-3d [17].



Scheme 1. The synthetic route of the SubPc derivatives.

2.2. Instruments and measurements

FT-IR spectra were recorded on a Nicolet spectrophotometer (KBr pellets). Mass spectra were obtained using a MALDI-TOF spectrometer (Bruker). H NMR spectra were acquired using a Bruker Ultrashield spectrometer. UV-Vis absorption and emission spectra were measured on a UV-2501PC spectrophotometer and an Edinburgh Instruments fluorimeter, respectively. Cyclic voltammetry (CV) was performed on a CHI 640E system with a three-electrode setup.

2.3. OPD device fabrication and characterization

Prior to deposition, ITO-coated glass substrates were sequentially ultrasonicated in deionized water, acetone, and ethanol (30 min each) followed by UV-ozone treatment for 20 min. A 40-nm-thick PEDOT: PSS hole-transport layer was deposited by spin-coating (2000 rpm, 30 s) and thermally annealed at 100°C for 20 min. The active layer was prepared by spin-coating (2000 rpm, 30 s) a blended solution of SubPc: PVK (1:4 wt %) in 1, 2-dichlorobenzene under nitrogen atmosphere, yielding a 40-nm film after annealing at 90°C for 15 min. Finally, a 30-nm C₆₀ electron-transport layer and a 1-nm LiF interlayer were thermally evaporated at rates of 0.3 nm / s and 0.1 nm / s, respectively. Finally, a 120 nm aluminium layer was deposited at a rate of 3 nm / s, thus completing the fabrication of the UV photodetector.

The photoresponse characteristics, such as on-off switching curves and response times, were acquired on a Keithley 2400 source meter. Impedance spectroscopy was performed with a Zahner Ennium electrochemical workstation.

3. Results and discussions

3.1 Photophysical properties

Figure 1(a) displays the normalized absorption spectra of the four SubPc derivatives and each derivative exhibits a distinct high-energy absorption band within the UV region, specifically between 290 and 320 nm. Notably, as the solvent polarity increases, the axial substituents of the subphthalocyanine compounds do not significantly alter the positions of the maximum absorption peaks. In Figure 1(b), a bathochromic shift is observed in the maximum emission wavelengths, which could be attributed to the electron-donating nature of the axial phenoxy substituent. These groups destabilize the HOMO energy level, leading to the observed redshift [11]. Additionally, the B-band absorption of the SubPc compounds shifts to longer wavelengths, likely due to enhanced π -conjugation resulting from the axial phenoxy substitution [18].

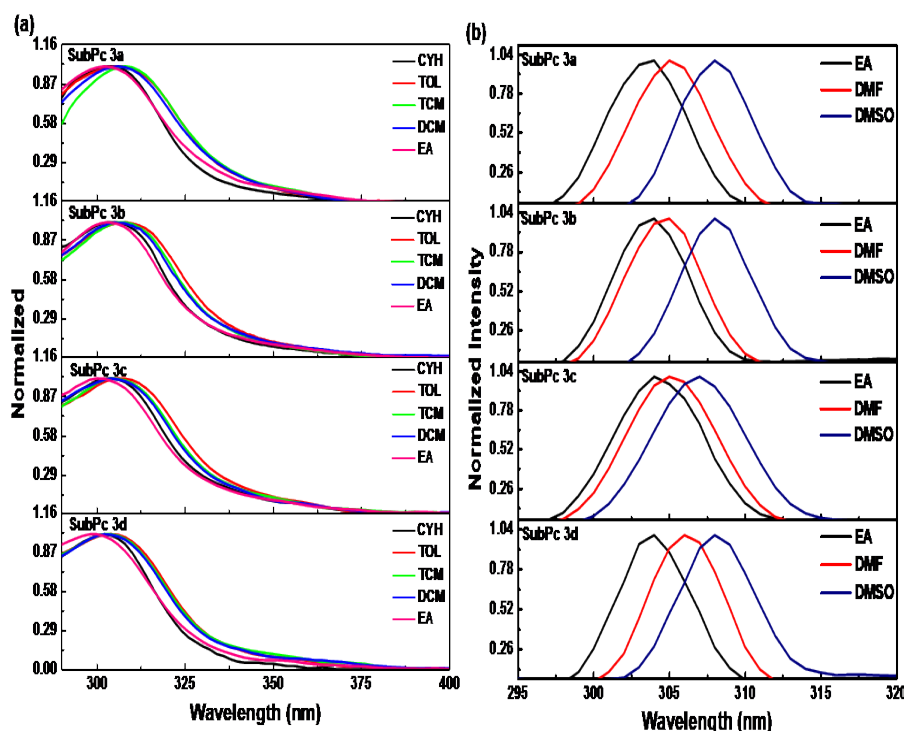


Fig. 1. (a) Absorption spectra and (b) fluorescence of SubPc solutions: 1) Cyclohexane (CYH), 2) Toluene (TOL), 3) Chlorobenzene (PhCl), 4) Chloroform (TCM), 5) dichloromethane (DCM) 6) Ethyl acetate (EA), 7) *N,N*-Dimethylformamide (DMF), 8) Dimethyl Sulfoxide (DMSO).

3.2. Thermal properties

We tested the thermal stability of SubPc derivatives 3a–3d using thermogravimetric analysis (TGA) under a nitrogen atmosphere at a heating rate of 30 °C per minute. The curves, exhibited in Figure 2, indicate that all four compounds are very stable at temperatures below 100 °C, with only a small weight loss of less than 10 %. However, these materials exhibit significant thermal decomposition at temperatures exceeding 180 °C, during which their molecular frameworks collapse into smaller fragments [19]. This behaviour underscores their thermal limitations and provides critical insights into their stability under high-temperature conditions.

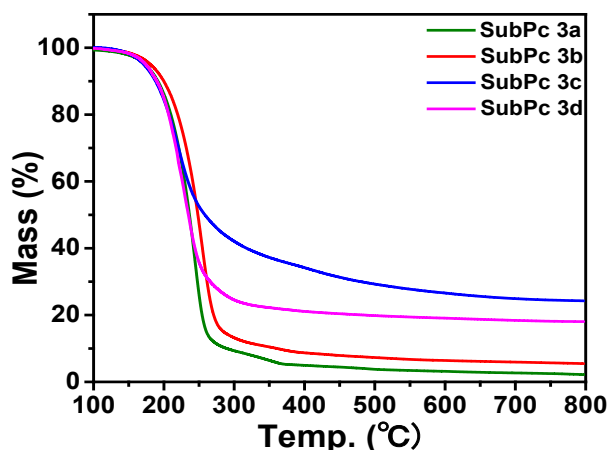


Fig. 2. TGA curve of SubPc 3a-3d.

3.3. Electrochemical properties

To evaluate the energy levels of the synthesized SubPc derivatives, we performed cyclic voltammetry (CV) using a CHI640E electrochemical workstation. The measurements were conducted by a standard three-electrode system in a tetrahydrofuran (THF) solution (1×10^{-4} M) and used tetrabutylammonium hexafluorophosphate (Bu_4PF_6) as supporting electrolyte. The assembly consisted of a platinum wire counter electrode, a polished glassy carbon working electrode and a double-junction Ag/Ag^+ reference electrode. The resulting CV curves and electrochemical data, presented in Figure 3 and Table 1, reveal useful information about the electronic properties of these compounds.

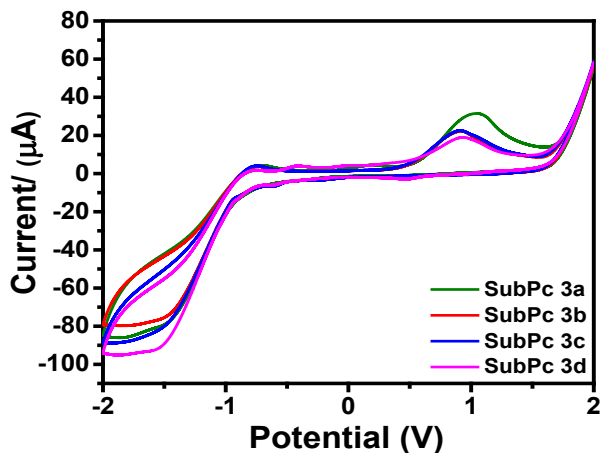


Fig. 3. CV curves of SubPc derivatives in THF.

Table 1. Electrochemical dates of SubPc derivatives.

SubPc	$E_{\text{ox}}^{\text{[a]}}$ (V)	HOMO ^[b] (eV)	$E_{\text{g}}^{\text{[c]}}$	LUMO ^[d]
SubPc	1.05	- 5.79	2.19	- 3.60
SubPc	0.92	- 5.66	2.20	- 3.46
SubPc	0.90	- 5.64	2.20	- 3.44
SubPc	0.90	- 5.64	2.23	- 3.41

[a] Oxidation onsets were determined from cyclic voltammetry measurements. [b] HOMO energy levels were calculated using: $\text{HOMO (eV)} = - (4.74 + eE_{\text{ox}})$ eV (relative to vacuum level). [c] Optical band gaps (E_{g}) were derived from UV-Vis absorption edge wavelengths (λ_{onset}): $E_{\text{g}} \text{ (eV)} = 1240/\lambda_{\text{onset}}$. [d] $|\text{LUMO}| = |\text{HOMO}| - E_{\text{g}}$.

As shown in Table 1, the four SubPc derivatives have optical energy gap E_{g} values of 2.19 – 2.23 eV and HOMO energy level values of -5.79 – -5.64 eV, which are close to typical electron donor materials [20]. This indicates that these compounds are more suitable as donor materials for organic photodetectors.

3.4. Theoretical calculation

We used the Gaussian 16 package to optimize the SubPc derivative geometrical configuration via density-functional theory (DFT) and employed the B3LYP method and the 6-31G (d) basis set. The optimized geometries, illustrated in Figure 4, demonstrate the influence of axial phenoxy substitution on the molecular orbital (MO) energy levels. The calculated HOMO and LUMO energy levels are consistent with the electrochemical measurements (Table 1), with frontier orbital distributions predominantly localized on the subphthalocyanine ring for SubPc 3a-3c. This indicates that the electron-withdrawing axial substituents have negligible impact on the orbital distribution. In contrast, SubPc 3d exhibits a distinct behavior, with its frontier orbital primarily concentrated on the axial substituents. The observed elevation of both HOMO and LUMO levels relative to other derivatives stems from the strong electron-donating character of the axial amino substituent.

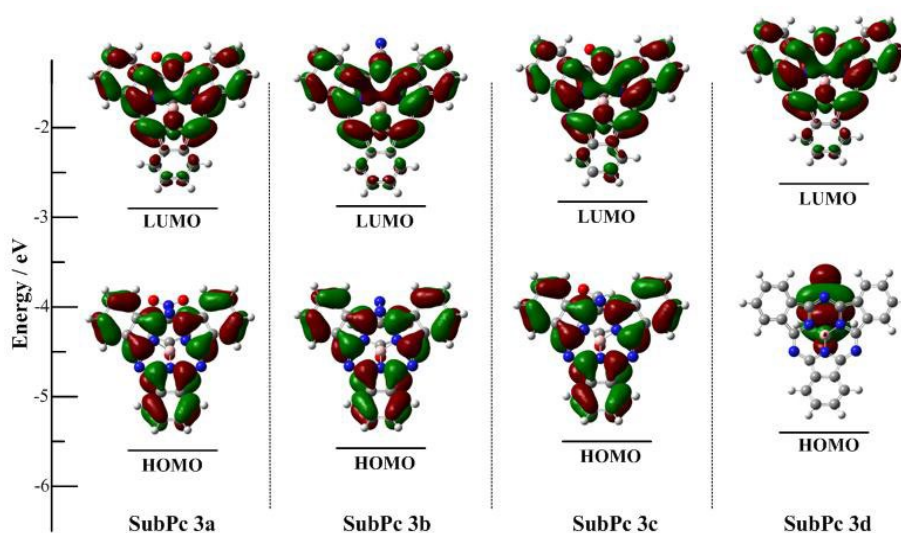


Fig. 4. Effects of four compounds on MO energy levels

3.5. Photodetection properties

The structure of the device is composed of an ITO anode, a PEDOT: PSS hole injection layer, an active layer formed by blending SubPc derivatives with a minor proportion of PVK, a C₆₀ electron transport layer, and a LiF/Al cathode, as illustrated in Figure 5. The addition of PVK markedly improves the film-forming capabilities of the SubPc derivatives, while maintaining transparency in the UV spectrum, rendering it highly suitable for applications in UV photodetection.

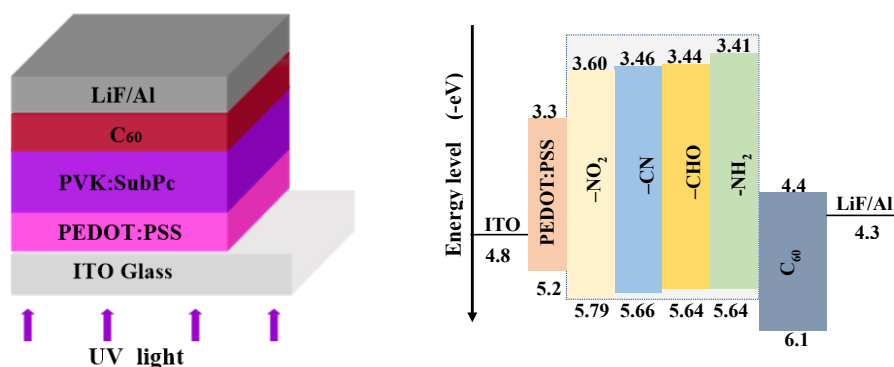


Fig. 5. Device structure diagram of four compounds.

The photocurrent performance of the photodetectors was assessed under 320 nm UV light exposure at 0 V, as depicted in Figure 6. The measured photocurrents at on-state for devices utilizing SubPc 3a, 3b, 3c, and 3d were 2.43, 2.01, 1.46, and 0.62 μ A, respectively. Notably, the SubPc 3a-based photodetector exhibited a significantly enhanced photocurrent generation of 1.81 μ A compared to the SubPc 3d device under identical illumination conditions. Repeated on/off cycles demonstrated that the subphthalocyanine photodetectors exhibit consistent and stable responses to UV light, highlighting their reliability.

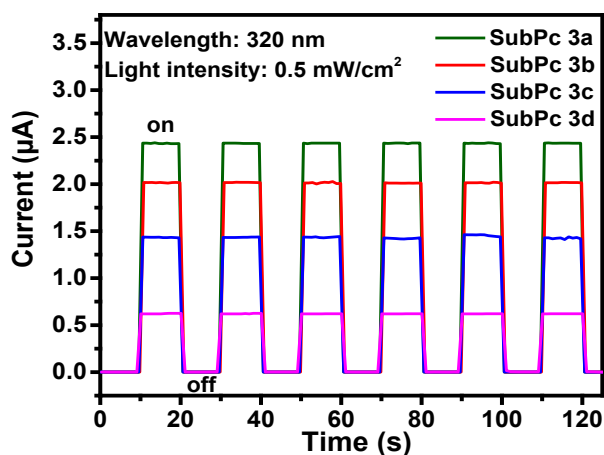


Fig. 6. Switching characteristics of the SubPc-based photodetectors.

To further characterize the photodetectors, key performance parameters such as R , D^* and EQE were calculated using the following formulas [21, 22]. These parameters are summarized in Table 2.

$$R = \frac{\Delta I}{A \times P} \quad (1)$$

$$D^* = \frac{R}{\sqrt{2qJ_d}} \quad (2)$$

$$EQE = \frac{R \times hc}{e\lambda} \quad (3)$$

Here, ΔI represents the disparity between the photocurrent and the dark current (derived from Figure 6), A signifies the effective device area, P represents the incident light intensity, q stands for the charge of an electron, J_d indicates the dark current density, h is Planck's constant, c is the speed of light, e is the elementary charge, and λ corresponds to the incident light wavelength.

Table 2. Photodetector performance metrics (0 V Bias).

Devices	Light intensity	Detectivity		Sensitivity	
		I_{light} (μA)	D^* ($\text{cm} \cdot \text{Hz}^{1/2}/\text{W}$)	R (A/W)	EQE (%)
SubPc 3a	320 nm	2.47	2.18×10^{12}	12.35×10^{-2}	38.76
SubPc 3b	0.5 mW/cm^2	2.01	1.78×10^{12}	1.78×10^{-2}	31.54
SubPc 3c		1.43	1.26×10^{12}	1.26×10^{-2}	22.45
SubPc 3d		0.62	0.54×10^{12}	0.54×10^{-2}	9.73

Response time (τ) is one of the key parameters that determine the ability of photodetectors to track rapidly changing optical signals. Figure 7 shows the response times of these four photodetectors, whose response time is 32, 32, 32, and 37 ms respectively. It is demonstrated that the four photodetectors can detect weak light and respond quickly to ultraviolet light.

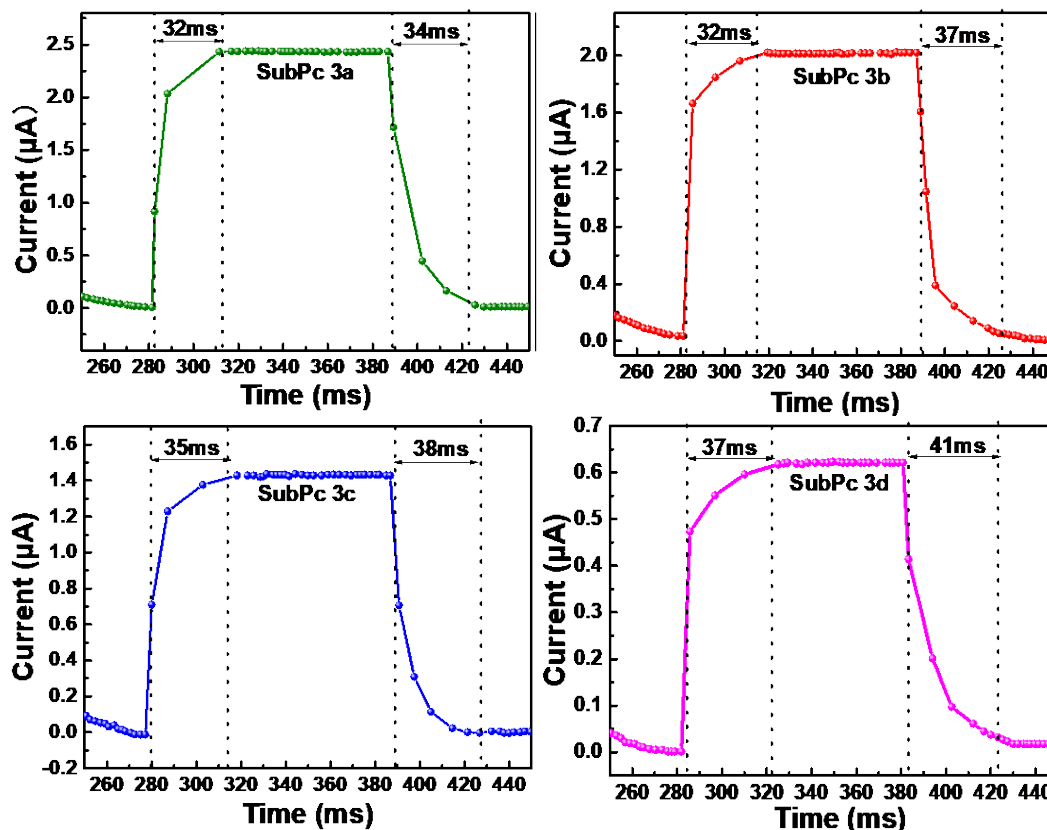


Fig. 7. The diagrams of the light response times of the four photodetectors based on SubPcs.

To further elucidate the impact of different axial substituents on the conductivity of the devices, impedance spectroscopy was employed. An equivalent circuit model, tailored to the device structure, was constructed to analyze the charge transfer resistance. The impedance spectra of the devices are presented in Figure 8. In the impedance spectra, the diameter of the semicircular region stands for the charge transfer resistance (R_p), while R_s represents the interface resistance across the PEDOT: PSS hole transport layer.

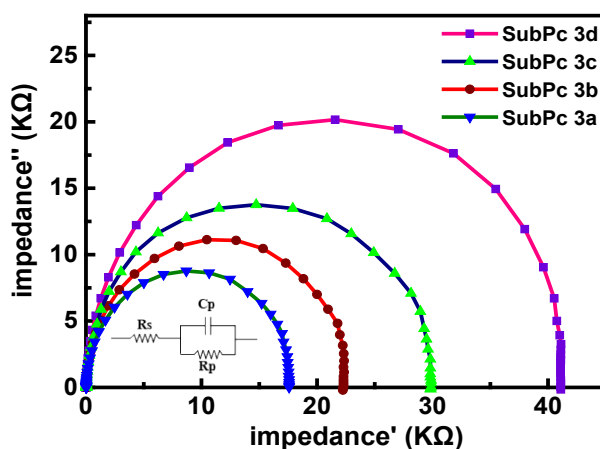


Fig. 8. Impedance spectra of the four SubPc-based photodetectors. The inset shows the equivalent circuit of the impedance model.

Additionally, R_p and C_p refer to the resistance and capacitance of the active layer, respectively. Among the four compounds, SubPc 3a exhibited the lowest impedance, indicating superior electron transfer and transport capabilities, while SubPc 3d showed the highest impedance and significantly lower conductivity. These findings highlight the critical role of axial substituents in modulating the electronic properties of SubPc derivatives.

4. Conclusions

This study demonstrates the potential of the synthesized SubPc derivatives as active layer materials for UV photodetectors, exhibiting excellent electrical conductivity and rapid response times. Under 320 nm UV illumination at zero bias, showed optimal performance, reaching a peak EQE of 38.76%, a D^* of 2.18×10^{12} Jones, and a fast response time ($\tau \approx 32$ ms). Its low impedance further confirms superior electron transport properties and enhanced electrical conductivity, contributing to its exceptional light detection capabilities. These results advance our understanding of SubPc derivatives for UV detection and provide some basis for their future development in optoelectronic devices.

Acknowledgements

This work has been supported by the College Student Innovation and Entrepreneurship Training Program Project (no. 202410060014) and National Natural Science Foundation of China (no. 21401138).

References

- [1] H. Chen, K. Liu, L. Hu, A.A. Al-Ghamdi, X. Fang, *Mater. Today* 18, 493 (2015); <https://doi.org/10.1016/j.mattod.2015.06.001>
- [2] A. F. McKinlay, *Health Phys.* 87, 171 (2004); <https://doi.org/10.1097/00004032-200408000-00006>
- [3] A. Hosseini, M. Abrari, S. S. Malvajerdi, S. M. Mohseni, H. D. Sun, M. Ghanaatshoar, *ACS Appl. Mater. Interfaces* 6, 22036 (2023); <https://doi.org/10.1021/acsanm.3c04218>
- [4] X. Y. Zhou, Z. H. Lu, L. C. Zhang, Q. Q. Ke, *Nano Energy* 117, 108908 (2023); <https://doi.org/10.1016/j.nanoen.2023.108908>
- [5] M. H. Jia, L. B. Tang, K. S. Teng, Y. F. Lü, *Appl. Surf. Sci.* 643, 158641 (2023); <https://doi.org/10.1016/j.apsusc.2023.158641>
- [6] D. Bhat, S. Sahoo, J. Bhattacharyya, D. Ray. *Org. Electron.* 87, 105975 (2020); <https://doi.org/10.1016/j.orgel.2020.105975>
- [7] D. Shao, W. Zhu, X. Liu, M. Li, J. Chen, Y.-Y. Sun, G. Xin, J. Lian, S. Sawyer, *ACS Appl. Mater. Interfaces* 12, 43106 (2020); <https://doi.org/10.1021/acsaami.0c09890>
- [8] Y. Bernhard, P. Richard, R. A. Decréau, *Tetrahedron* 74, 1047 (2018);

<https://doi.org/10.1016/j.tet.2018.01.029>

[9] P. J. Swarts, J. Conradie, *Inorg. Chem.* 59,7444 (2020);

<https://doi.org/10.1021/acs.inorgchem.0c00150>

[10] C. G. Claessens, D. Gonzalez-Rodriguez, T. Torres, *Chem. Rev.* 102, 835 (2002);

<https://doi.org/10.1021/cr0101454>

[11] W. Li, D. Li, G. Dong, L. Duan, J. Sun, D. Zhang, L. Wang, *Laser Photonics Rev.* 10, 473 (2016); <https://doi.org/10.1002/lpor.201500279>

[12] G. E. Morse, M. G. Helander, J. F. Maka, Z. H. Lu, T. P. Bender, *ACS Appl. Mater. Interfaces* 2, 1934 (2010); <https://doi.org/10.1021/am1002603>

[13] M. G. Helander, G. E. Morse, J. Qiu, J. S. Castrucci, T. P. Bender, Z. H. Lu, *ACS Appl. Mater. Interfaces* 2, 3147 (2010); <https://doi.org/10.1021/am100632y>

[14] T. Kawata, Y. Chino, N. Kobayashi, M. Kimura, *Langmuir* 34, 7294 (2018);

<https://doi.org/10.1021/acs.langmuir.8b01118>

[15] C. E. Mauldin, C. Piliago, D. Poulsen, D. A. Unruh, C. Woo, B. Ma, J. L. Mynar, J. M. J. Fr'echet, *ACS Appl. Mater. Interfaces* 2, 2833 (2010); <https://doi.org/10.1021/am100516a>

[16] P. J. Swarts, J. Conradie, *Electrochim. Acta.* 329, 135165 (2020);

<https://doi.org/10.1016/j.electacta.2019.135165>

[17] F. Ma, G. Zhang, X. Wu, W. Qu, Z. Sun, X. Li, X. Yin, *J. Phys. Chem. C* 126, 13496 (2022); <https://doi.org/10.1021/acs.jpcc.2c04232>

[18] Y. Wang, L. Zhu, T. Wang, Y. Hu, Z. Deng, Q. Cui, Z. Lou, Y. Hou, F. Teng, *Org. Electron.* 62, 448 (2018); <https://doi.org/10.1016/j.orgel.2018.08.017>

[19] X. Xu, X. Zhou, K. Zhou, Y. Xia, W. Ma, O. Inganäs, *Adv. Funct. Mater.* 28, 1805570 (2018);

<https://doi.org/10.1002/adfm.201805570>

[20] S. S. Maklakov, T. V. Dubinina, M. M. Osipova, E. F. Petrusevich, A. D. Mishin, L. G. Tomilova, *J. Porphyr. Phthalocya.* 20, 1 (2016); <https://doi.org/10.1142/S1088424616500759>

[21] D. González-Rodríguez, T. Torres, E. L. G. Denardin, D. Samios, V. Stefani, D. S. Correa, *J. Organomet. Chem.* 694, 1617 (2009); <https://doi.org/10.1016/j.jorganchem.2008.10.055>

[22] I. A. Skvortsov, U. P. Kovkova, Y. A. Zhabanov, I. A. Khodov, N. V. Somov, G. L. Pakhomov, P. A. Stuzhin, *Dyes and Pigments* 185, 108944 (2021);

<https://doi.org/10.1016/j.dyepig.2020.108944>